aerospace

MDPI

Article

Experimental and Numerical Investigation of Novel Acoustic Liners and Their Design for Aero-Engine Applications

Moritz Neubauer [1,*], Julia Genßler [2], Vincent Radmann [3,*], Fleming Kohlenberg [2], Michael Pohl [4], Kurt Böhme [1], Karsten Knobloch [5], Ennes Sarradj [3], Klaus Höschler [4], Niels Modler [1] and Lars Enghardt [2]

1 Institute of Lightweight Engineering and Polymer Technology (ILK), Technische Universität Dresden, Holbeinstraße 3, 01307 Dresden, Germany
2 Institute of Fluid Dynamics and Engineering Acoustics, Technische Universität Berlin, Müller-Breslau-Str. 8, 10623 Berlin, Germany
3 Institute of Fluid Dynamics and Engineering Acoustics, Technische Universität Berlin, Einsteinufer 25, 10587 Berlin, Germany
4 Chair of Aero Engine Design, Brandenburg University of Technology Cottbus-Senftenberg, Siemens-Halske-Ring 14, 03046 Cottbus, Germany
5 German Aerospace Center (DLR), Institute of Propulsion Technology, Engine Acoustics, Müller-Breslau-Str. 8, 10623 Berlin, Germany
* Correspondence: moritz.neubauer@tu-dresden.de (M.N.); vincent.radmann@tu-berlin.de (V.R.); Tel.: +49-351-463-4026

Abstract: This paper presents a combined experimental and numerical investigation on a novel liner concept for enhanced low-frequency and broadband acoustic attenuation. In particular, two different realizations, derived from conventional Helmholtz resonators (HR) and plate resonators (PR) are investigated, which both deploy flexible materials with material inherent damping. In this context, a comprehensive experimental investigation was carried out focusing the identification and evaluation of various geometric parameters and material properties on the acoustics dissipation and related properties of various materials in a simplified setup of a single Helmholtz resonator with flexible walls (FHR concept). Furthermore, a parameter study based on analytical models was performed for both liner concepts, taking into account material as well as geometric parameters and their effects on transmission loss. In addition, design concepts that enable cylindrical or otherwise curved liner structures and the corresponding manufacturing technologies are presented, while considering essential structural features such as drainage. With respect to the potential application in jet engines, a structural–mechanical analysis considering the relevant load cases to compare and discuss the mechanical performance of a classical HR and the FHR concept liner is presented. Finally, both concepts are evaluated and possible challenges and potentials for further implementation are described.

Keywords: acoustic liner; plate resonator; Helmholtz resonator; broadband noise; honeycomb structure; model; curved design

check for updates

Citation: Neubauer, M.; Genßler, J.; Radmann, V.; Kohlenberg, F.; Pohl, M.; Böhme, K.; Knobloch, K.; Sarradj, E.; Höschler, K.; Modler, N.; et al. Experimental and Numerical Investigation of Novel Acoustic Liners and Their Design for Aero-Engine Applications. *Aerospace* **2023**, *10*, 5. https://doi.org/10.3390/aerospace10010005

Academic Editors: Peng Wei and Rosario Pecora

Received: 2 November 2022
Revised: 2 December 2022
Accepted: 15 December 2022
Published: 21 December 2022

1. Introduction

Aviation generates various emissions (e.g., CO_2, NO_X and noise), which impact people's quality of life in the vicinity of airports and beyond. These emissions occur at all phases of the flight, with highest nuisance during take-off and landing. One way to reduce the noise emissions is to optimize the geometry of the fan, respectively the whole engine, which may interfere with contrary optimization requirements for fuel efficiency or other aircraft design criteria. Currently, an important part of the reduction of the emitted engine noise is obtained by liners (usually an array of cells covered by a perforate) installed in the nacelle intake and at other locations of the engine. To increase propulsive efficiency and reduce the gaseous emissions as well as the noise emissions, the increase of engine bypass ratios has proven to be very successful. While delivering the same thrust, larger fans rotate

slower than the smaller ones which leads to lower rotor-stator interaction frequencies. To reduce the emitted tonal and broadband noise, standard liners would require a larger volume and increased depth to address the tonal components at lower frequency, which is conflicting with the limited design space and aerodynamic requirements. Most standard liners for aero-engine applications consist of a perforated face sheet, which is attached to a lightweight core structure and a rigid back plate underneath. This type of liner is called a single-degree-of-freedom liner, as each cell can be modeled individually as a simple spring-and-mass system—usually considered as a Helmholtz resonator (HR). To extend their relatively small first resonance bandwidth, several concepts for multi-degree-of-freedom liners exist. These include multi-layer liners consisting of two cell layers with a septum or "mesh cap" in between [1–4]. While these concepts offer a more broadband damping, they cannot lower the system's first resonance frequency. In contrast, different concepts, such as folded cavities [1–4], active elements [5–8] or attached mass elements [6,9], offer the possibility for low frequency damping, with certain drawbacks and limitations connected to each of these concepts.

In the current study, two liner concepts, with improved noise attenuating characteristics, which use flexible elements with material inherent damping properties to address low-frequency noise, are investigated. Their acoustic performance is described by their dissipation or transmission loss of acoustic energy. Note, that in contrast to the liner impedance, these entities depend on the specific assembly situation. In Figure 1 the holistic approach of the investigation is shown, which includes the experimental and analytical modeling of the acoustic concepts as well as the structural mechanical analysis of different cell configurations. Additionally, feasibility studies on the design and manufacture of the liner structures were presented in order to assess the potential and challenges of integrating them into jet engines.

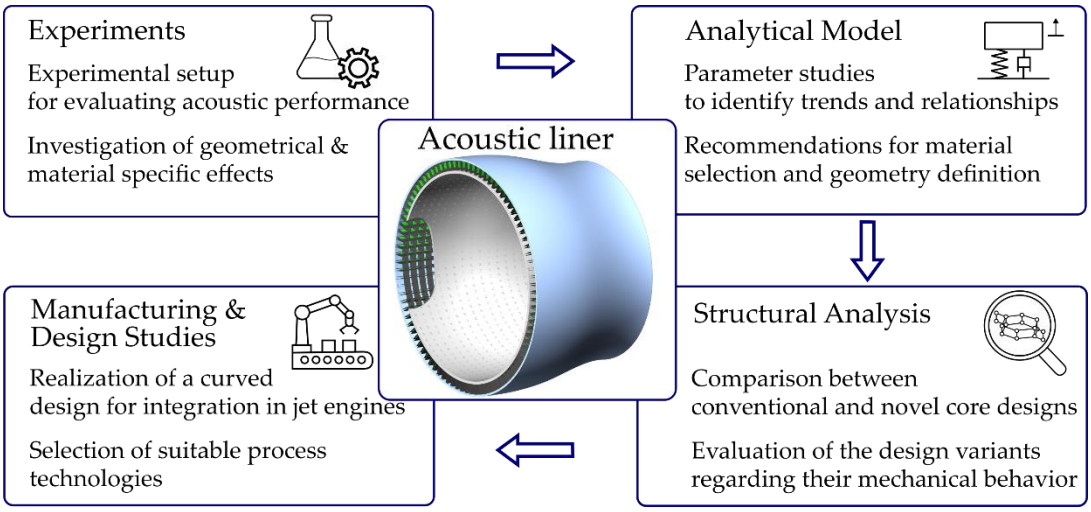

Figure 1. Holistic approach of the presented research to analyze novel acoustic liners concepts considering experimental, analytical modeling, structural mechanical and manufacturing aspects.

For the first concept, the FHR concept, the aim is to combine the high acoustic dissipation of the standard HR with the low frequency geometric resonance of a flexible plate by the use of flexible walls and a back cavity. While the Helmholtz resonator has been investigated widely, including analytical, experimental and numerical investigations, the combination with one or more flexible walls changes the system drastically and requires different analytical description or boundary conditions for numerical simulations.

The second concept deploys a plate resonator (PR) silencer that consists of an expansion chamber fully covered by a plate [10,11]. In addition to the ability to attenuate low-frequency noise with low depth cavities, plate silencers have the advantage over porous absorbers or HR structures with perforated surfaces that they can be exposed to

contaminated air without any agglomeration of contaminants in the cavity. Furthermore, their flow resistance is very low due to the smooth surface [12]. Beside other applications, plate silencers are used in air conditioning systems to reduce the noise emission through the pipework or in industrial ventilation systems [13,14]. Currently, the most advanced model to describe the acoustic behavior of a plate silencer was introduced by Huang and Wang [15,16]. It describes the interaction of the system of cavity and plate with the duct above. Thereby, the performance significantly depends on the plate material [17]. To adjust a suitable frequency range and bandwidth, different materials and resonator dimensions are under investigation, without a comprehensive and accurate design process being available so far.

A well-designed aero-engine liner excels in damping acoustical pressure waves but also withstands mechanical pressure and is safe and reliable. Due to their lightweight structure, liners usually consist of sandwich honeycomb core structures. The research dealing with their safety and reliability focuses on the mechanical behavior of these structures. The examined cores in those studies are usually made out of aramid paper [18–21]. Giglio et al. [22] applied a Finite Element Analysis (FEA) simulation to determine the crush mechanics for a Nomex core and showed a high-fidelity simulation. Liu et al. [23] evaluated the impact of bonding imperfections under flatwise core compression of layered cell walls. They investigated that the de-bonding causes out-of-plane stresses inside the wall. The behavior of hybrid honeycomb structures, consisting of flexible and rigid wall areas, under axial compression was also analyzed using FEA [24]. The results indicate not a stability failure of the entire structure but material failure on the micro and meso level. Besides the honeycomb core, there are also other core structures, such as the folded core [25] or the X-type lattice structure [26]. However, for the intended application, the design with square honeycombs is more relevant. In this context, Cote et al. [27] investigated the impact of sandwich walls in contrast to monolithic walls and got the result of improved through-thickness compressive strength. In contrast to the previous studies, the present work improves the understanding of the effects of the change in core geometry due to the integration of flexible films.

Many applications of honeycomb cores in functional sandwich structures, such as acoustic liners, require a curved shape, in particular for instance the geometry of the intake of a jet engine. However, sandwich cores are mainly manufactured planar and subsequently formed into the desired shape, which potentially causes damage of the composite, malfunction and geometric change of the cells [28–31]. In this context, alternative processes are necessary for the manufacturing of the resonator configurations considered here comprising flexible walls to enable also curved design applications. This process needs to ensure the geometric integrity of the resonator and especially the film. For the manufacturing of the strip slotted design of cell cores introduced by Dannemann et al. [32], built of fiber-reinforced plastic, a productive cutting process as abrasive water jet or laser milling is needed to efficiently manufacture the face sheets and cell walls from flat panels [33]. In addition, the deep drawing process enables highly efficient forming of fiber-reinforced thermoplastic woven and knitted fabrics for load-bearing cell chambers, which are well-suited for the production of cavities, especially for the PR liner concept [34–36]. With regard to the process of joining the cavity and the flexible films made of thermoplastic materials, there is the potential to apply welding technologies, such as ultrasonic welding, to realize high joint strengths at high speed and low cost even without energy direction transmitters [37,38]. In this context, studies that specifically investigated the weld-ability of the targeted material polyamide 6 with glass fiber reinforcement (PA6-GF) imply that fiber-reinforced polyamide 6 (PA6) requires significantly less energy than unreinforced PA6 to achieve high joint strengths [39,40].

In the following sections, comprehensive experimental results for a modular mock-up of the novel FHR are presented. Subsequently, the acoustic performance of the PR silencer as well as the FHR was evaluated by using semi-analytical models for each concept. In order to compare the mechanical performance of both designs, the structural–mechanical

analysis of a classical HR and the FHR liner are conducted and discussed. With regard to the application of the two acoustic liner principles in aerospace, design concepts that enable a curved design and the corresponding manufacturing technologies are presented. Finally, a conclusion and an outlook for further investigations are drawn.

2. Acoustic Analysis of Helmholtz Resonator with Flexible Walls and Results

2.1. Experimental Setup for the HR

In order to investigate several design parameters and parameter dependencies of the FHR concept, acoustic measurements were performed in the DUCT-R facility of the DLR in Berlin. The facility consists of a rectangular duct with the liner test section in the middle and microphone sections upstream and downstream of the test section (see Figure 2). For the excitation of acoustic waves with and against the mean flow, a loud speaker is attached on the upstream and downstream end of the tunnel, respectively. The sound waves are excited either via speaker A or speaker B with a single tone and an amplitude of 110 dB, ensuring a linear regime for the periodic in- and outflow at the considered perforate. The microphones (five in the upstream and five in the downstream section) are non-equidistantly attached to the duct wall to avoid singularities in the wave decomposition needed to calculate the scattering coefficients. The measured frequency range is 204–1020 Hz in steps of 26 Hz and from 1071 Hz to 2040 Hz in steps of 51 Hz. Since the main dissipation peaks of the investigated liner are expected below 1000 Hz, smaller step sizes were selected in this frequency range. The cut-on-frequency of the first higher mode in the hard wall section is 2142 Hz, thus only plane waves are investigated in the present study. The anechoic terminations at both ends of the DUCT-R reduce end reflections and improve the accuracy of the measurements. For more information about the test rig and wave decomposition, see [41]. The rectangular shape of the DUCT-R allows the attachment of planar resonators, that are easier to manufacture than curved ones and therefore more suitable for basic studies.

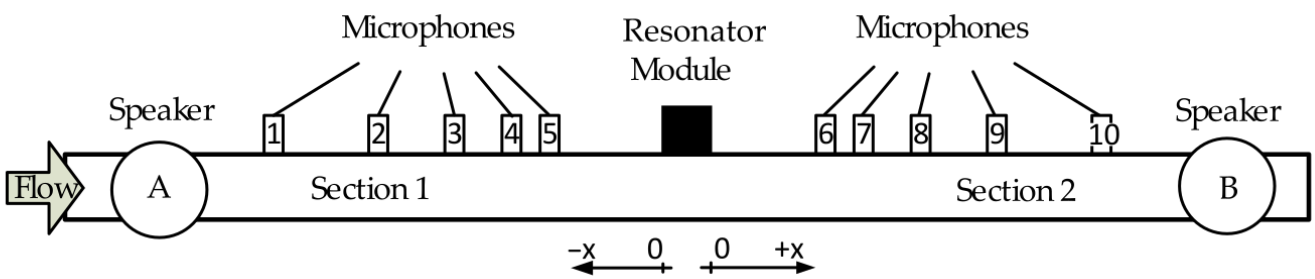

Figure 2. Schematic view of the DUCT−R test rig.

To investigate the interactions between an HR and a flexible wall, a small modular resonator was developed consisting of a resonator body that allows various elements, such as flexible walls, to be attached to its five remaining sides. The additional elements are connected to the main body via threaded rods. The basic structure for this investigation consists of a main resonator with a flexible wall and a back cavity attached to it. The flexible walls are made out of different materials with different thicknesses and are clamped between aluminium metal plates with distinctive cut-outs. Ten screws ensure a clamped boundary condition. The other six holes visible in the plate holder (Figure 3b) are used for the mounting on the threaded rods. The shape of the flexible element between resonator and back cavity is determined by the cut-out shape. Several basic shapes were investigated: round (diameter: 15 mm), square (side length: 15 mm) and rectangular (side length: 15 × 26 mm). A plate holder with a mounted flexible plate with a square cut-out is shown in Figure 3b.

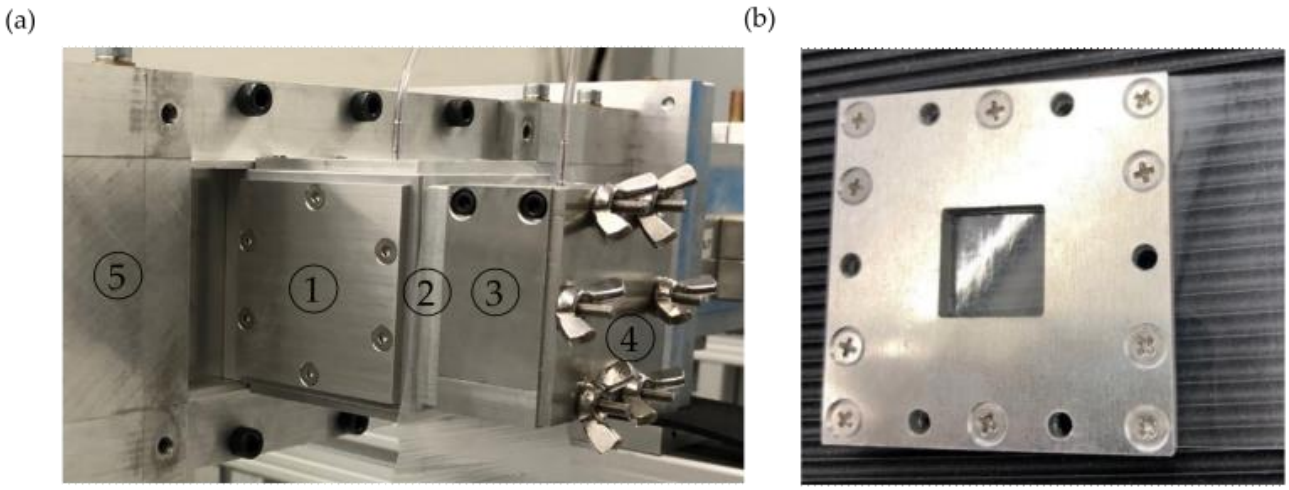

Figure 3. (**a**) ① Assembly of resonator, ② holder with film, ③ back cavity (here ~0.5 of resonator volume) and ④ back plate at the ⑤ DUCT-R; (**b**) holder with square cut-out and (TPU) film.

Two different sizes of back cavities were built in order to vary its volume. One back cavity is as large as one-quarter of the resonator volume, the other is about one-half of the resonator volume. The parts can be combined to form back cavities with a volume of one-quarter, one-half, three-quarters up to twice the resonator volume. The back cavity is closed by another aluminium plate with a thickness of 3 mm. This back plate is assumed rigid and fastened by wing nuts as shown in Figure 3a. The resonator is attached to the test section of the DUCT by a perforated face sheet. In the area of the resonator, the face sheet has 18 holes with a diameter of 1.5 mm each. The resonator has a square area of 35×35 mm^2 and a depth of 50 mm when used as a normal Helmholtz resonator. This configuration of the resonator exhibits a Helmholtz resonance between 600–700 Hz. The one-quarter wave resonance frequency due to the cavity depth would be 1715 Hz but is altered by the presence of the face sheet yielding the above Helmholtz resonance frequency. The walls and back cavities can be attached parallel or orthogonal to the DUCT-R main axis and to each other due to the nearly cubical form. The presented modular setup therefore offers the possibility to change the shape of the flexible wall; the material and thickness of the flexible wall; the position of the flexible wall with respect to the resonator (and thereby the main duct); the size of the back cavity; and the number of flexible walls and back cavities attached to the main resonator. The investigated materials with their Young's modulus and different thicknesses are shown in Table 1.

Table 1. Measured film materials with their Young's modulus and thicknesses.

Thickness mm	Aluminum (Alu) 70,000 MPa	Poly Propylene (PP) 1600 MPa	Thermoplastic Polyurethan (TPU) 16 MPa	Polyamide 6 (PA6) 800 MPa	Polyphenylene Sulphide (PPS) 2400 MPa	Polyether Ether Ketone (PEEK) 2800 MPa
0.001	x					
0.01	x	x	x		x	x
0.02		x				
0.03			x			
0.04				x		

2.2. Results of Experimental Investigations of the FHR Design

The measurement results clearly show that the integration of a flexible wall has an impact on the resonance of the resonator system (see Figure 4a). With regard to the possible variations of the modular resonator, the flexible wall made of TPU material had the greatest impact on the dissipation of the resonator system. Compared to a simple HR with the same overall volume (cavity + back cavity), the resonator with an additional flexible wall has

a higher resonance frequency as shown in Figure 4a. Adding a back cavity changes the effect of the flexible wall in the dissipation. This means that, by adding a back cavity, the main dissipation shifts slightly to higher frequencies, and an additional dissipation peak at lower frequencies occurs. This additional peak is strongly dependent on the material and thickness of the flexible wall (Figure 4a) as well as dependent of the back cavity size (Figure 4b). Using a flexible wall of polypropylene (PP) the dissipation is slightly widened around the Helmholtz frequency. All the other materials tested showed no effect on the Helmholtz frequency. This may be due to their comparatively high Young's modulus, as the materials appear to be "acoustically stiff".

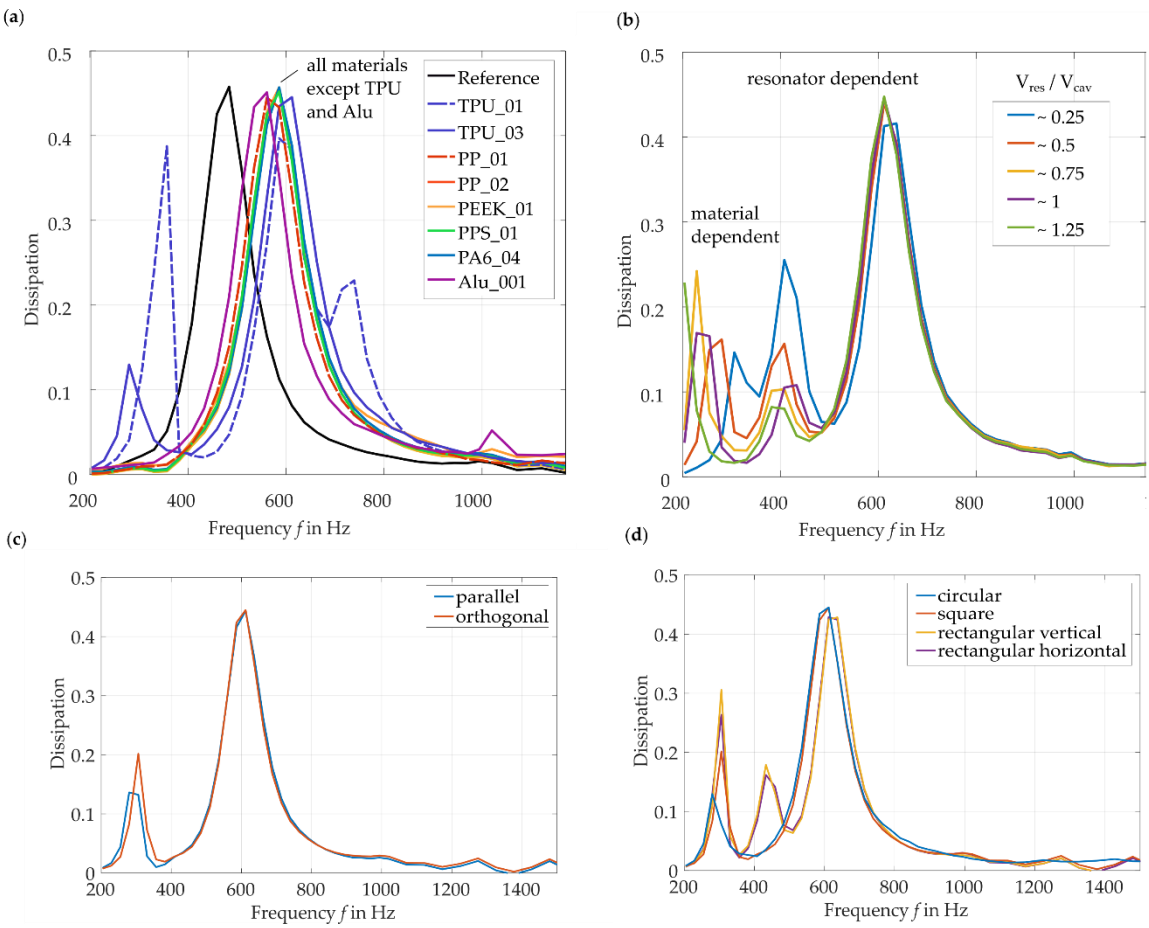

Figure 4. Comparisons of different aspects in the dissipation in dependence of (**a**) materials and thicknesses (constant back cavity and circular shaped cut-out), (**b**) the size of the back cavity in relation to the resonator volume (same material and rectangular shaped cut-out), (**c**) orientation of the back cavity in relation to the Duct (same material and circular shaped cut-out) and (**d**) the shape of the cut-out (TPU_03 and same back cavity size).

Besides the material, the film thickness also has a great impact on the acoustic performance. This holds especially true for the flexible wall made out of TPU. While the thin TPU film (0.1 mm) shows a high secondary dissipation peak but involves difficulties in reproducible mounting, the thicker TPU film (0.3 mm) is easier to apply and has easier reproduction of results. Furthermore, the tension of the mounted film affects the dissipation. Measurements conducted with the thicker TPU film still showed a dependency on the applied tension during assembly. The film was bent prior to acoustic excitation, and the dissipation was altered significantly, if a torque higher than 0.2 Nm was applied to fasten the screws. In more than 50 repetitions of mounting, this sensitivity caused both higher and lower frequencies for the material dependent dissipation peak. Therefore, the

reproducibility of the mounting process is important regarding the manufacturing process of the liner.

The size of the back cavity has an impact on the additional dissipation peak, especially when using the flexible wall made out of TPU. A linear trend is visible for the dissipation peak around 400 Hz (see Figure 4b). The material dependent dissipation (see Figure 4b) depends on the material itself as well as on the flexible walls shape (compare Figure 4d) and the depth of the back cavity. This effect becomes evident in Figure 4b, where the first peak of material dependent dissipation occurs at around 400 Hz. The lower frequency peaks seem to be dependent on the depth of the back cavity and the shape as it also occurs with the round and rectangular shape. However, there is a slight shift in both frequencies for the curve of $V_{res}/V_{cav} = 1$, which does not correlate with the observed trend for other cavity sizes. This shift can be explained by a different thickness distribution over the investigated film area, which is caused by the manufacturing process.

The position of the flexible wall in relation to the DUCT main axis has no influence on the dissipation (compare Figure 4c). Therefore, it can be concluded that the orientation of back cavity and Helmholtz cavity is interchangeable. This fact is important for the liner sample geometry for future investigations. The slight difference in the first peak in Figure 4c could be due to a manufacturing-related variation in thickness of the used film material specimens and does not limit the above conclusion.

The cut-out shape also has an influence on the dissipation. In this context, the rectangular cut-out shows a distinct dissipation with two peaks while, for the circular or square cut-out, there is only one peak (Figure 4d). Note that the width of the square cut-out is equal to the diameter of the circular cut-outs. The rectangular cut-out, however, has different lengths of 15 × 26 mm. Since the rectangular cut-out has two distinct dimensions, compared to one for the circular and square cut-out, two distinct resonances are visible.

To gain a better understanding of the trends observed in the experiments, parameter studies were performed for both the FHR and PR liner concepts. Their modeling and results are presented in the following section.

3. Semi-Analytical Parameter Studies for FHR and PR Liner Concepts

Parameter studies are a reasonable way to correctly understand the behavior of FHR and PR liners. However, only a limited number of cases can be investigated with measurements. Therefore, semi-analytical approaches are used in the following to conduct several parameter studies. Thus, it is possible to evaluate the influence of the most important geometrical and material-specific parameters for the FHR and the PR liner concept. The experimental investigations from the previous section showed that materials with a low Young's modulus are needed for resonances in the investigated frequency range between 200 and 1500 Hz. In light of these results, only thermoplastics and thermoplastic elastomers were considered for the parameter studies in order to restrict the parameter range to one material group. For these materials there exists a functional relationship between the Young's modulus E and the loss factor η as shown in [17]:

$$\eta = 0.0355 \cdot E^{-0.633}, \text{with } E \text{ in GPa.} \quad (1)$$

This functional relationship effectively reduces the parameter space dimensions by one. The baseline values for both resonator concepts are shown in Table 2. Based on these values, one parameter after the other is varied to highlight the main trends.

Table 2. Values of geometry and material parameters.

Parameter	Symbol	Unit	Value, Value Range	Design Point
Common parameters for both concepts				
Duct height	h_d	mm	60	60
Duct width	w_d	mm	∞	∞
Young's modulus	E	MPa	$E \in [10^1; 10^4]$	14
Poisson ratio	ν	-	0.48	0.48
Loss factor	η	-	$\eta \in [0.65; 0.008]$	0.53
Density	ρ	kg/m^3	1080	1080
Plate thickness	h_p	mm	$h_p \in [0.1; 0.5]$	0.3
FHR specific parameters				
Plate diameter	d_p	mm	$h_p \in [12; 18]$	15
Cell cross Section	A_{cell}	mm^2	19×19	19×19
Face sheet porosity	σ	-	2.6%	2.6%
Face sheet thickness	h_{fs}	mm	2	2
Main cavity height	h_{mc}	mm	40	40
Second cavity height	h_{sc}	mm	$h_{sc} \in [5; 20]$	10
Liner length	l_{liner}	mm	200	200
PR specific parameters				
Cavity length	l_c	mm	$l_c \in [30; 90]$	65
Cavity height	h_c	mm	$h_c \in [5; 35]$	30
Cavity width	w_c	mm	∞	∞

The transmission loss (TL) is a commonly used parameter to characterize silencers and is used in this work as the target variable to quantify the performance of both liner concepts. The transmission loss describes the acoustic effectivity of a liner, and following [42], it is calculated from the ratio of the transmitted sound power P_t and the incident sound power P_i:

$$TL = -10 \log_{10} \left| \frac{P_t}{P_i} \right|. \tag{2}$$

Note that the TL does not indicate whether the losses are due to reflection or dissipation. Conversely, a very reflective and a very dissipative silencer both yield a high transmission loss, while only the latter has a high dissipation (as energy is just reflected back to the source but not converted into heat). The TL was chosen in our parameter studies since it is a commonly used parameter to characterize silencers and offers the comparability of the acoustic performance of both concepts. The following results for both liner concepts are presented as color maps. These color maps can be read as topographic maps of the transmission loss over frequency for each varied parameter (or in the case of the Young's Modulus and loss factor, parameter pair). Slicing the color map horizontally leads to the frequency spectrum of transmission loss of a single value—respectively, a value pair—of the varied parameter. The lighter areas depict the peaks of the transmission loss and therefore areas where the liner performs best.

3.1. Result and Discussion of Parameter Studies for the FHR Concept

Following the experimental setup from the previous section, the configuration consists of cells with a main cavity, which is connected to a second cavity by a flexible plate and attached to the duct channel by a perforated face sheet. A sketch of the single cell is depicted in Figure 5. Note that the single cell was extended to multiple cells with a total liner length l_{liner} of 200 mm to better highlight the results. This is admissible as the single cell is locally reacting.

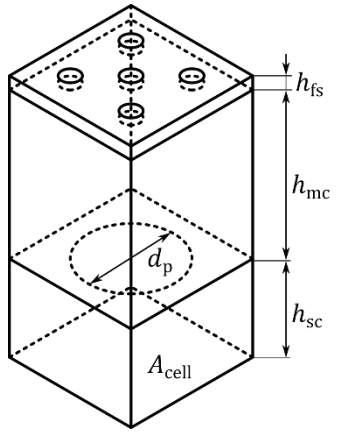

Figure 5. Schematic view of a single FHR cell.

The analytical modeling of the FHR concept is based on the works of Kohlenberg et al. [9], where the modeling was introduced and verified using experimental data. It combines one dimensional waveguide theory with lumped elements. The idea is to start at the thermal boundary layer at the back of the resonator and use a waveguide model to spatially transform that impedance through the resonator up to the channel. The flexible plate is modeled as an equivalent impedance and integrated into the waveguide model. The result is an overall impedance of the resonator system where the interaction of the cavities and the flexible wall together form a Multi-Degree-Of-Freedom system. Therefore, it is incorporated in the successive transformation of impedances. The flexible plate is assumed to be round, clamped and only vibrating in its first mode. With these assumptions, an equivalent impedance is calculated and integrated into the waveguide model. The result is an impedance of the resonator system, which is used as a boundary condition in a numerical simulation, which solves the Helmholtz equation to predict scattering coefficients including the TL and the dissipation of the duct section with the resonator system attached to one side. The results of the parameter studies of the Helmholtz resonator system with flexible walls are summarized in Figure 6.

The parameter studies revealed that the frequency dependent TL of the liner is strongly dependent on the Young's modulus (and thereby also the loss factor) of the flexible plate (see Figure 6a). Two peaks are visible in the low elastic region. The lower frequency peak starting from around 550 Hz can be attributed to the plate resonance. The second resonance frequency starting from around 900 Hz is due to the Helmholtz resonance between the face sheet and main cavity. With increasing Young's modulus, the plate resonance increases as well. This is expected since only the first clamped circular mode is taken into account with a resonance frequency of

$$\mathrm{f}_{\mathrm{eig,plate}} \sim \mathrm{Re}\left\{ \frac{h}{d^2} \cdot \sqrt{\frac{E(1+\mathrm{i}\eta)}{\rho}} \right\}, \tag{3}$$

with h the plate thickness, d the plate diameter and ρ the plate density. Note that the resonance frequency of the system attributed to the plate resonance is not the same as the in vacuo resonance frequency represented in Equation 3. This is because the overall resonance behavior depends on the plate as well as on the cavities dimensions. In the modeling they are linked through the combination of their respective impedances. The relationship regarding the plate resonance inside the resonator system is not presentable in a satisfying analytical form, hence we conducted parameter studies to show this behavior discretized. In contrast to the resonance associated with the plate resonance, the Helmholtz resonance hardly changes up to a transition zone around $E = 100$ MPa. In this transition zone, the transmission loss peak attributed to the plate's resonance rises sharply with increasing Young's Modulus. For very stiff plates ($E = 10^3$ MPa) only one transmission loss peak

is visible. In this configuration the flexible plate acts as a rigid back wall and only the Helmholtz resonance is visible. To dampen low frequency noise, materials with a low Young's modulus are therefore preferred.

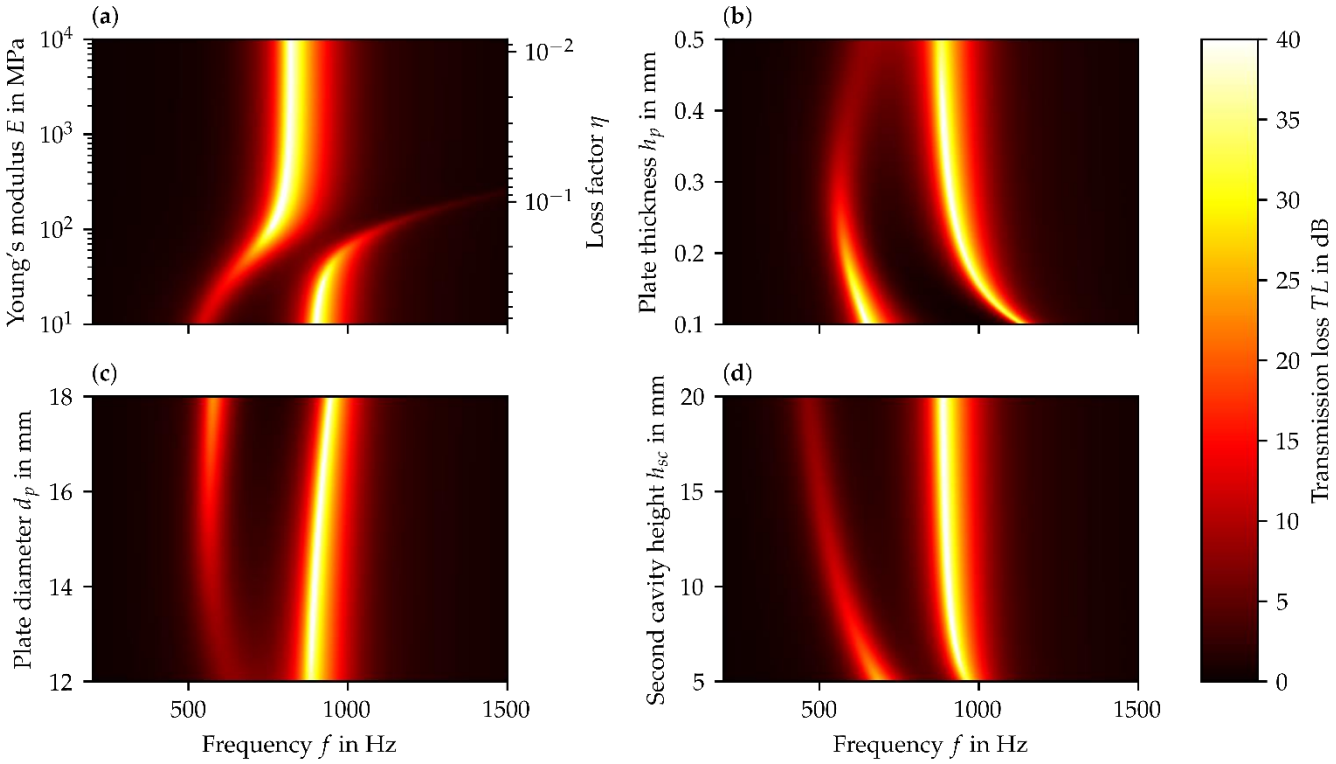

Figure 6. Results of the parameter study of the Helmholtz resonator with flexible walls, (**a**) variation of Young's modulus E and loss factor η, (**b**) variation of plate thickness h_p, (**c**) variation of plate diameter d_p, (**d**) variation of second cavity height h_{sc}.

The plate thickness has a strong impact on the TL as well (see Figure 6b). For very thin plates, three effects are visible: First, the higher TL peak associated with the Helmholtz resonance is altered towards higher frequencies. Second, the frequency of the TL peak due to the plate resonance decreases up to a thickness of around 0.3 mm which is in contrast to Equation 3, where the in-vacuo resonance increases linearly with the plate thickness. Thus, the plate's behavior with respect to the plate thickness inside the resonator system differs from the in-vacuo case. For thicker plates, the resonator system tends to show only one TL peak associated with the Helmholtz resonance. This can be explained by the fact that a very thick plate approaches a rigid back wall. A thin plate is consequently preferable for a strong attenuation of noise with low frequency components.

In contrast to the previous depicted parameters, the TL is altered in its amplitude but not in its frequency with respect to a variable plate diameter (see Figure 6c). For small flexible plates, the Helmholtz resonance seems to dominate the spectrum. For large diameters, the flexible plate enables a higher TL at lower frequencies. The plate diameter thus needs to be as big as possible to put the flexible plate effectively into use but is limited by the dimensions of the cavity. However, as the plate resonance gets stronger, the Helmholtz resonance is shifted towards higher frequencies. In comparison to the parameter study regarding Young's modulus (see Figure 6a), the system seems to be insensitive regarding the plate diameter. However, it must be considered that the variation of the elastic modulus includes several decades.

Finally, the influence of the second cavity depth regarding the TL was investigated (see Figure 6d). The Helmholtz resonance seems to be largely independent of the second cavity depth greater than 10 mm but is slightly altered to higher frequencies for very shallow

second cavities. The TL peaks associated with the plate-cavity sub-system is highest for small second cavity depths, yet the resonance frequency is anti-proportional to the depth. As nacelle space for aero-engine applications is very limited, a smaller second cavity is thus advisable.

3.2. Result and Discussion of Parameter Studies for PR Liner Concept

Furthermore, parameter studies were carried out with the PR liner. The applied semi-analytical model (see Figure 7) was initially developed by Huang and Wang [15,16]. It describes a two-dimensional PR liner with a simply supported plate. A simple PR liner is composed of a duct and a wall mounted thin plate facing the duct and closing a cavity behind it. The flexible plate is excited by the sound propagating along the duct, which causes a pressure difference above and below the plate. Thus, the vibrating plate interacting with the cavity dissipates one part of the incoming sound energy, and another part is reflected back in direction of the sound source. The validity of the model has already been demonstrated in former publications [43,44]. Furthermore, this model has already been used to conduct parameter studies to investigate the acoustic performance of the plate silencer. These researchers investigated, for example, the effects of the plate material on the transmission loss and the approximation quality of the model [10,12,17,45].

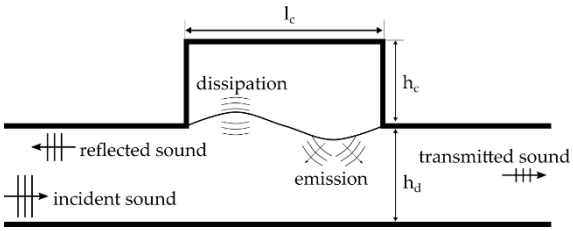

Figure 7. Sketch of a simple plate silencer.

The parameter studies presented here are based on the geometric and material specific values in Table 2. The results show the frequency dependent TL for different parameter variations in form of a color map (Figure 8). Different from the FHR, the PR model provides the results for one chamber and not for an entire liner consisting of several chambers in series. This must be taken into account when evaluating the absolute transmission loss values. Varying Young's modulus (and correlated the loss factor), the TL appears with increasing Young's modulus in clear s-shaped patterns, and between them more and more distinctive discontinuities occur. This behavior corresponds to an eigen frequency shift from higher to lower odd modes of the plate and is also discussed in [17]. However, in addition to the direct relationship between Young's modulus and plate resonances, there is also an interaction with the cavity below, which can affect the frequency of the plate resonance. Another effect, which can be observed, is the blurring of the s-shaped patterns with increasing loss factor and more distinct and brighter shapes with increasing Young's modulus. This implies that the peaks of the TL become narrower and higher as the Young's modulus becomes higher. Otherwise, the peaks become wider and flatter as the loss factor increases. Furthermore, it can be seen that the s-shaped patterns cause one or two peaks to appear in the TL over the frequency spectrum. Thus, one or two TL peaks can be obtained by the choice of material as well as the width of these peaks.

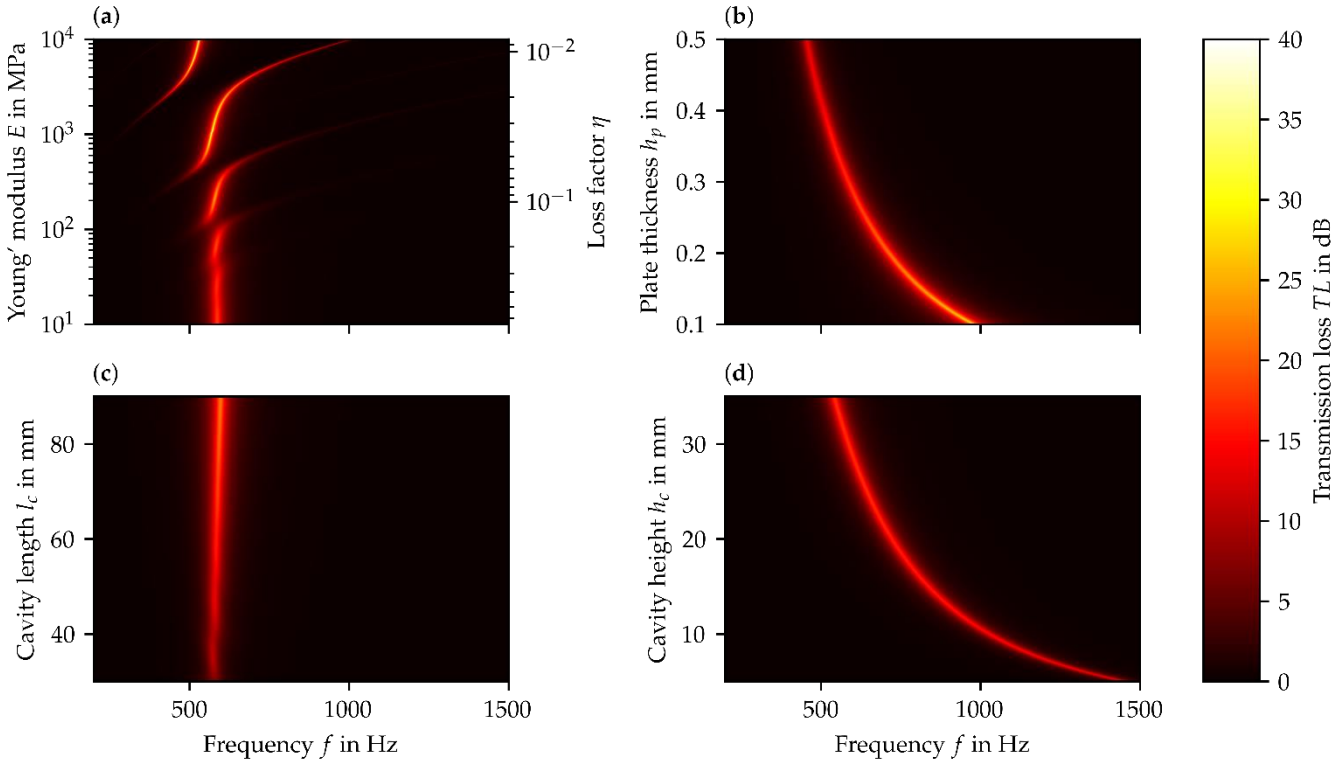

Figure 8. Results of the parameter study of the plate silencer, (**a**) variation of Young's modulus E and loss factor η, (**b**) variation of plate thickness h_p, (**c**) variation of plate length l_p, (**d**) variation of cavity height h_c.

Furthermore, the results show that the plate thickness h_p has a very strong impact on the location of the TL maximum (see Figure 8b). It can be seen that a thicker plate results in attenuation at lower frequencies. Thereby, the maximum TL converges to approximately 500 Hz. Thus, it does not seem possible to attenuate even lower frequencies with an even thicker plate. In addition, thicker plates result in lower absolute transmission loss. In the extreme case, the duct wall and the flexible plate would approach each other, resulting in the loss of the desired TL. However, the bandwidth of the TL is barely influenced by the plate thickness. Moreover, the s-shaped patterns caused by the plate modes cannot be observed here. This is due to the selection of the design point with a comparative high loss factor.

The length of the plate and cavity l_c has a much smaller impact on the frequency of the maximum TL (see Figure 8c). There is only a minimal shift to higher frequencies with increasing plate length observable. This parameter has a more obvious influence on the absolute TL, which increases significantly with increasing plate length. Furthermore, it leads to slightly more broadband attenuation.

To influence the frequency of the maximum TL, the cavity height h_c has the biggest impact (see Figure 8d). Thus, a cavity height between 5 and 35 mm covers a frequency range of almost 1000 Hz. The frequency of maximum TL decreases with increasing cavity height but approaches 500 Hz asymptotically for the considered PR liner configuration. A higher cavity also broadens the TL peak slightly, but a significantly higher attenuation is not achieved.

The application of the FHR or PR concept as a liner in jet engines requires not only acoustics but also structural mechanics and manufacturing investigations, which are presented in the following chapters.

4. Structural Mechanics Analysis and Results

The application of an acoustic liner does not merely depend on the acoustical performance but also on its ability to withstand the conditions during the operation inside a jet engine. It is crucial to determine the maximum load capacity of each component to ensure the reliability of the acoustic liner throughout its intended life cycle. In this context, a study was conducted to compare the mechanical properties between a conventional HR liner and a novel FHR liner with flexible films integrated in its side walls.

4.1. Structural Design

The conventional HR liners consist of a perforated face sheet, a back plate and a bioinspired honeycomb core structure with a high specific modulus suiting the strict requirements in aviation (Figure 9a) [46,47]. In the present study the conventional core is compared to an alternative core structure comprising square cells (Figure 9b). Due to the comparatively larger areas of the side walls and the less complex manufacturing and joining process, square combs hold an advantage for the integration of flexible films. The change in the geometry of the cell and the implemented cut-outs for the flexible films as well as the selection of a new combination of materials leads to miscellaneous mechanical properties that need to be considered for the application of maximum loads, which the liner has to withstand.

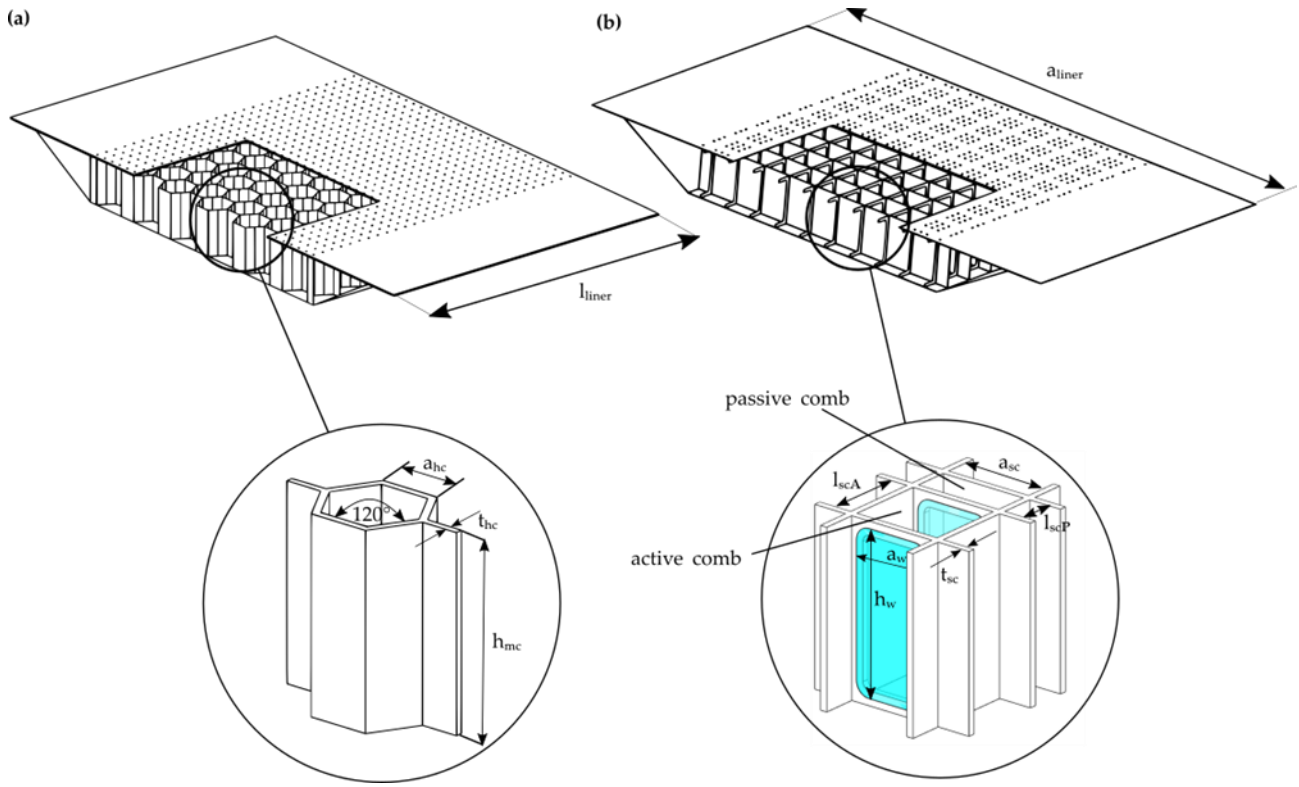

Figure 9. (**a**) Conventional HR liner and detailed honeycomb, (**b**) Resonator liner with square honeycombs detail of the square cells with film (turquoise).

In the course of this study, three configurations of the core design of the FHR Liner were compared. The first configuration (HR liner) represents the standard liner with a honeycomb core structure, made out of Carbon Fiber Reinforced Polymer (CFRP), Glass Fiber Reinforced Polymer (GFRP) and Nomex. The second and third configuration have a different core structure with square cells. The second configuration has the same materials and stack ups as the standard liner. The components of the third type are completely made out of PA6-GF. The components and the corresponding materials of the three design configurations are listed in Table 3. In order to enable a more accurate comparison with the

HR liner, the chamber volume of the rectangular core was converted to hexagonal shape for an initial preliminary investigation.

Table 3. Structure component, corresponding materials and thickness of the acoustic liner configuration.

Component	Face Sheet	Core	Back Plate		Cell Geometry	Mass [kg]
HR liner	2/2 Twill Weave * CFRP (0.2 mm)	Aramid Paper (Nomex) (0.194 mm)	10 UD-plies CFRP Orientation: $[0/0/45/90/-45/_s]$ (1 mm)	2 UD-plies GFRP Orientation: $[0/90]$ (0.2 mm)	Honeycomb	0.218
FHR-Type 1					Square Cells	0.240
FHR-Type 2	PA6-GF–2/2 Twill Weave (1 mm)	PA6-GF–2/2 Twill Weave (1 mm)	PA6-GF–2/2 Twill Weave (1 mm)	PA6-GF–2/2 Twill Weave (1 mm)	Square Cells	0.573

* diagonal appearance by a two-by-two weave where two warp yarns float over two weft yarns.

4.2. Materials

Apart from the geometry, a variation of different materials is considered for the components of the three configurations. In this context, the core of the conventional acoustic liner (HR and FHR-Type 1) consists of aramid paper (Nomex) and a face sheet and back plate, which are made out of carbon fiber and glass fiber reinforced epoxy resin. In contrast, the structure of the novel liner concept (FHR-Type 2) is made entirely of PA6-GF. In Table 4, the properties for each material are listed, including the detailed listing of the orthotropic material behavior and the consideration of different values in each load direction of unidirectional plies and woven plies.

Table 4. Material properties of the acoustic liner components.

Material	Nomex with Phenolic Resin	PVC-Rigid Foam Core	Carbon Fiber with Epoxy Resin–Unidirectional-(Woven Fabric)	PA6-GF E-Glass	Glass Fiber with Epoxy Resin
Youngs Modulus E_1 [MPa]	6034	70	129,000 (61,000)	18,000	29,700
Youngs Modulus E_2 [MPa]	5263	70	7380 (61,000)	18,000	29,700
Youngs Modulus E_3 [MPa]	4427	70	7380 (6900)	22,000	8600
Poisson's ratio ν_{12}	0.316	0.3	0.319 (0.04)	0.17	0.17
Poisson's ratio ν_{13}	0.327	0.3	0.319 (0.3)	0.17	0.17
Poisson's ratio ν_{23}	0.317	0.3	0.4 (0.3)	0.49	0.17
Shear Modulus G_{12} [MPa]	2142	27	4480 (3300)	7692	5300
Shear Modulus G_{13} [MPa]	1588	27	4480 (2700)	7692	3070
Shear Modulus G_{23} [MPa]	1865	27	2636 (2700)	7382	3070
Density ρ [kg/m^3]	1185	60	1560 (1420)	1800	2200
Fiber processing type	-	-	Unidirectional (Twill Weave 2/2)	Twill 2/2	Twill 2/2
Stress limits					
Tensile Strength $R_1^{(+)}$ [MPa]	62.3	1.5	2553 (805)	380	367
Tensile Strength $R_2^{(+)}$ [MPa]	48.2	1.5	42 (805)	380	367
Tensile Strength $R_3^{(+)}$ [MPa]	48.2	1.5	42 (50)	-	128
Compression Strength $R_1^{(-)}$ [MPa]	−85	0.96	1239 (509)	-	549
Compression Strength $R_2^{(-)}$ [MPa]	−78	0.96	199 (509)	-	549
Compression Strength $R_3^{(-)}$ [MPa]	−78	0.96	199 (170)	-	39
Shear strength R_{12} [MPa]	71.8	0.93	138 (125)	64	97
Shear strength R_{13} [MPa]	71.8	0.93	138 (65)	64	97
Shear strength R_{23} [MPa]	71.8	0.93	138 (65)	64	97

4.3. Modeling and Numerical Implementation

In order to analyze and compare the behavior of the three different liner structures, an FEA was carried out by using the simulation program (Ansys Workbench 2022 R.1., Ansys, Canonsburg, PA, USA). For the definition of the woven and unidirectional plies, the Ansys composite prepost (ACP) was used, allowing the specification of the fiber orientations and the stack-ups for each component according to Table 3. Since the thickness of each component is significantly lower than its length and width, shell elements of the type SHELL 181 were used. The convergence of the results occurred with an element size of 0.7 mm with a quadratic basis function and 8 nodes (Quad8). The resulting models were investigated in the course of a linear static–structural–mechanical analysis. Furthermore, the Tsai-Wu criterion [48] was applied to investigate the failure behavior of the composite structure for each component.

4.4. Constraints and Load Cases

In order to define the boundary conditions, a 3D Model was built for each core type (Table 3) and provided with the prevailing restrictions based on the application of acoustic liners in aero-engines. Typically, an acoustic liner is mounted on both sides in the axial direction of the engine to the inner nacelle structure. Since the liners applied in the inlet sections are rather short and the applications of screws lead to unfavorable aerodynamic conditions, an adhesive bonding or a clamp connection is preferred. In the bypass duct, the liners are additionally supported with screw connections due to their length. Therefore, the displacements on both sides are assumed to be fixed in all directions (see Figure 10). The green surfaces embody the fixed areas without displacement. To support the back plate, its bottom face (blue) is connected to a stiffer structure underneath the liner. For the simulation a friction free connection was chosen to prevent the liner from lifting off of the support structure in x_3-direction [26]. The common manufacturing process of acoustic liners leads to an adhesive bonding between the core structure, foam [47] core, back plate and face sheet. The sheets of each part were therefore implemented as a compound. Further, it is assumed that the integrated films have no significant influence on the stiffness of the FHR-Liner structure. Therefore, they are neglected in the CAD-Model and the simulation.

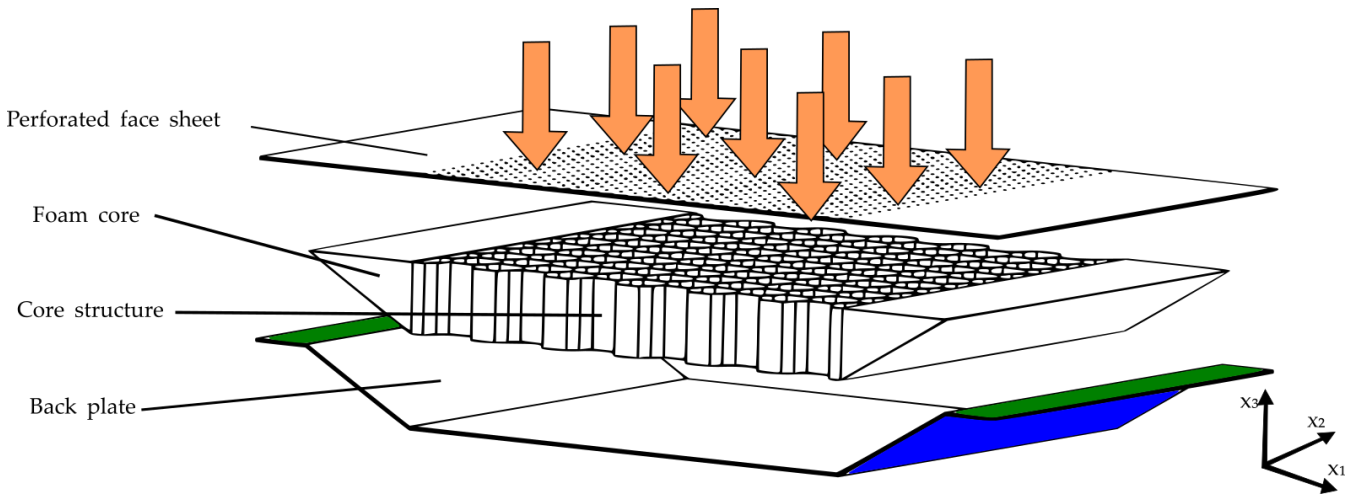

Figure 10. Fixed boundary condition (green), adhesive bonding (blue), applied forces (orange).

This study is limited to the two static load cases subjected to the acoustic liner during the life of an engine:

- global pressure loads due to pressure differences between the face sheet and the back side of the back sheet
- local loads due to maintenance

The maximal considered global pressure load during normal operation of the engine is 0.07 MPa. Typical local loads depict for example the set of footsteps during maintenance on the perforated face sheet. The load cases are applied normal to the face sheet along the x_3-axis (see Figure 10). The global pressure induced higher stresses and was therefore applied in the FEA.

4.5. Results of the FEA

In order to assess the effect of the variation in the core structure and the application of different materials, the three liner models were analyzed. The numerical analysis (Figure 11) shows the load influence of the face sheet. To determine the failure, a material exposure indicator is used. The so-called inverse reserve factor is ranging from 0 to 1, whereby 1 and above indicates the occurrence of failure and zero an unloaded condition. The value in the area of the face sheet for the HR-Liner (Figure 11a) is around 0.3. In contrast, for the FHR-Type 1 (Figure 11b), the value exceeds 1 and the failure of the fiber can be expected due to tensile stresses at the transition between face sheet and core wall in the area between the passive and active cell. The maximal deformation occurs in the middle of the active cell and nearly doubles between the honeycomb and square cell with the same material properties. Still, the novel liner has an increase in mass of around 10% (Table 3). The change in the core structure of an acoustic liner leads with the chosen material to a failure of the perforated face sheet. The application of the PA6-GF for the face sheet and Nomex core shows a much stiffer behavior (Figure 11c). However, this is associated with an increase of the total mass by nearly 100% compared to the standard.

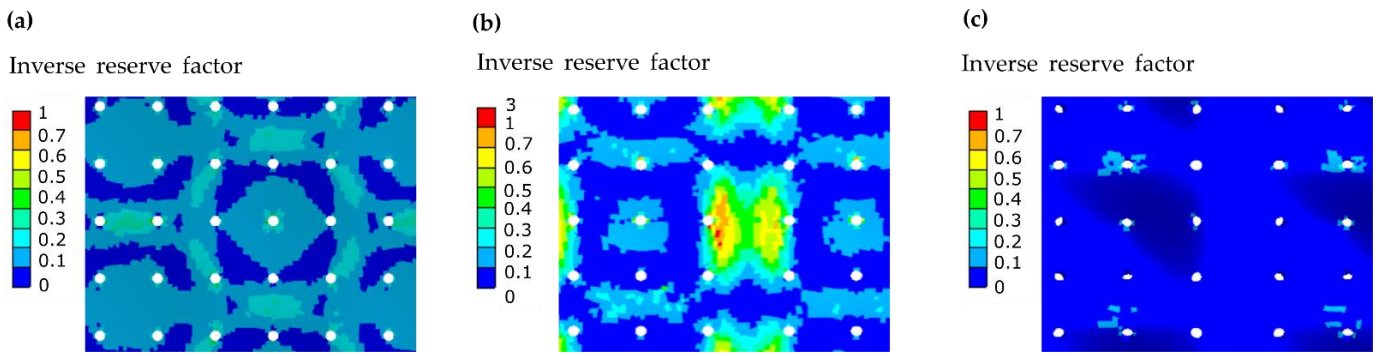

Figure 11. Workload of the perforated face sheets of the liner models (**a**) HR liner, (**b**) FHR liner with carbon fiber, (**c**) FHR liner with PA6-GF.

The application of the novel liner concept requires a cut-out inside the supporting core structure (Figure 9b). The influence of cut-out size and corner rounding on the mechanical properties was examined by Höschler et al. [49]. The investigations were carried out on the assumption that there are only active cells. The concept revision consisting of an active and passive cell leads, however, to a significant change for the load conditions inside the core. The changing order of walls with cut-outs and walls without cut-outs affect the force distribution and relieve the upper web of the frame. Depending on the distance l_{scP} of the passive cell, a reduction of the occurring stresses is evident. Figure 12 shows the correlation of the cell size and the maximum principal stresses for the FHR-Liner type 1. It is noticeable that the stress decreases with a decrease of the distance l_{scP}, while the size of the active cell remains the same. The deformation also decreases to the same extent.

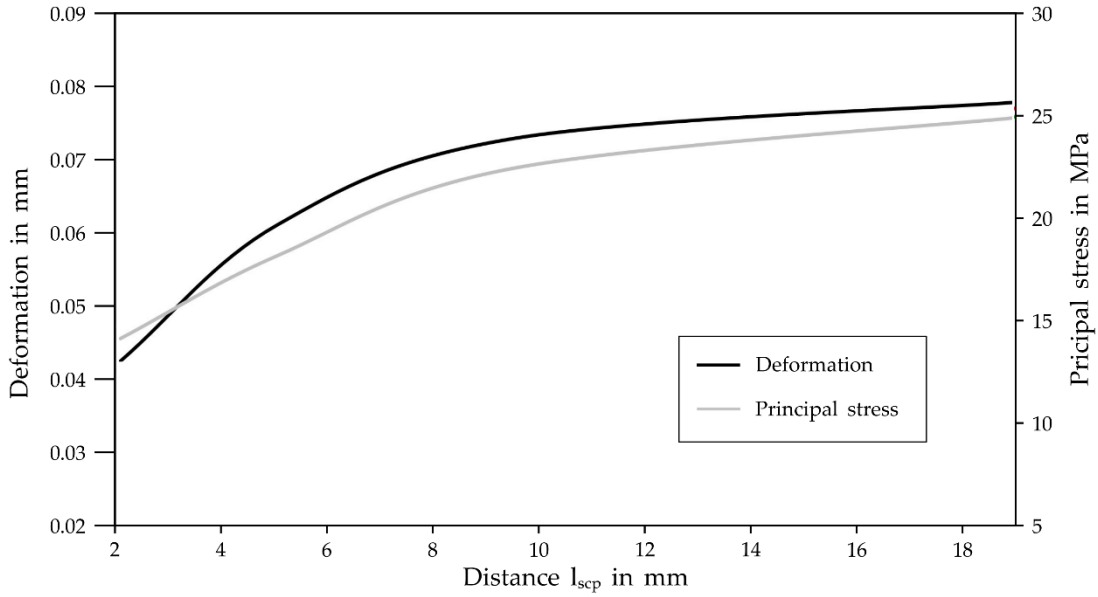

Figure 12. Change in stress and strain for different passive cell spacings.

Simultaneously, the weight of the liner increases as an increasing number of walls are necessary to cover a certain axial length l_{liner}. The maximum stresses and the largest deformations occur in the upper region for both HR and FHR liner. However, due to the cut-out, the stresses and deformations are higher for the FHR configuration. The combination of smaller spacing of the passive cell walls (see Figure 12) and the change of the material to PA6-GF results in significantly lower stresses in the cut-out frame (Figure 13c). Dependent on the chosen configuration, the thickness can be reduced and therefore the total weight of the FHR-liner. Figure 13d shows an increase in stress for the HR-Liner type 2 while reducing the spacing, the material thickness and the weight by 40% compared to the configuration of Figure 13c.

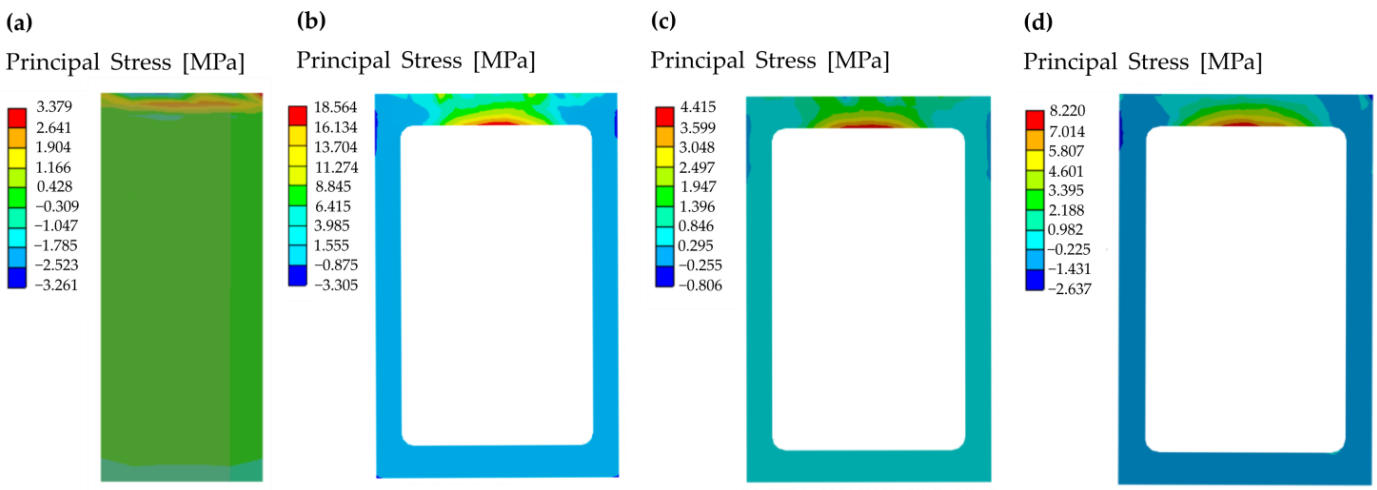

Figure 13. Distribution plot of the principal stresses of the core walls for the (**a**) HR-Liner; (**b**) FHR-Liner type 1; (**c**) FHR-Liner type 2 with $t_{sc} = 1$ mm and $l_{scP} = 5$ mm; (**d**) FHR-Liner type 2 with $t_{sc} = 0.25$ mm and $l_{scP} = 5$ mm.

5. Design and Manufacturing Feasibility Study for Curved Acoustic Liners

To evaluate the potential and challenges associated with the realization of curved acoustic liners for integration into jet engines, the following feasibility study was conducted. Given the film material is a key component in the introduced FHR and PR liner principles

in terms of acoustic performance, it is important to avoid compromising the geometry and bearing conditions of the films by implementing the curved shapes for the intended applications in jet engines. Since most of the currently used fabrication methods implement the curvature of the general liner structure in a way that can cause severe damage to the acoustic structure, a new design and corresponding fabrication methods are introduced in the following.

5.1. Design and Manufacturing Concept HR-Liner

The targeted design of the curved HR-Liner is based on the design introduced by Dannemann et al. [32]. The curved frame and rectangular stringer with cut-outs are manufactured using a laser or water jet cutting process (see Figure 14). In order to enable the necessary deflection of the film, an acoustically active cell, connected to the duct via perforations in the face sheet, and a passive cell without perforations are arranged alternately along the perimeter. This creates a pressure gradient between the cavities that allows the film material to deflect. In this context, for the passive cells, the slots of the frame should be closer together to decrease their volume and consequently increase the ratio of the acoustically active cells to the overall area covered.

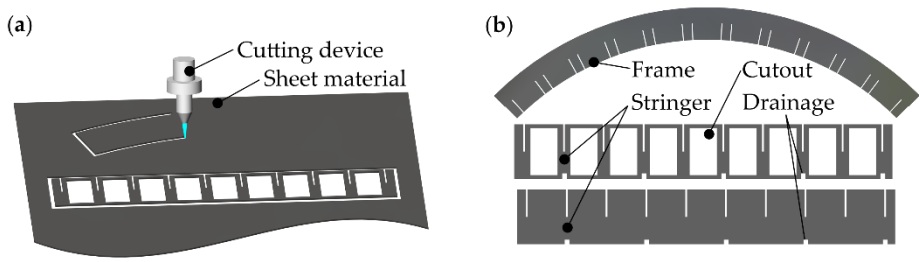

Figure 14. (**a**) Process of cutting the components of the resonator cavity out of sheet material, i.e., water jet or laser cutting, (**b**) curved frame with slits, the stringer with and without cut-outs for the flexible film.

According to previous studies and the experimental investigations presented before in this work, the stress state of the film is a pivotal constrain due to its impact on the damping characteristic of the liner [32]. In this context, the goal is to reproducibly pre-tension the film in the form that a subsequent joining process with the support structure without wrinkles but a defined stress state of the film is possible. For this purpose, the film is cut in the form of a biaxial specimen, clamped at the edges of the tabs and is force-controlled deflected by weights applied to the tabs. Subsequently, a fixing frame is used to conserve the films pretension state. In order to utilize the thermoplastic material properties of the film and the support structure while saving additional adhesives, the ultrasonic welding process is proposed for joining the two components. As shown in Figure 15b, the fixing frame is positioned and mounted on top of a lower support carrying the stringers with cut-outs. Then a windowed die, used to minimize the impact of the welding process on the conserved stress state of film, is mounted within the frame. In the next step, a rectangular sonotrode welds the film onto the stringers at a web width of 2 mm around the cut-out.

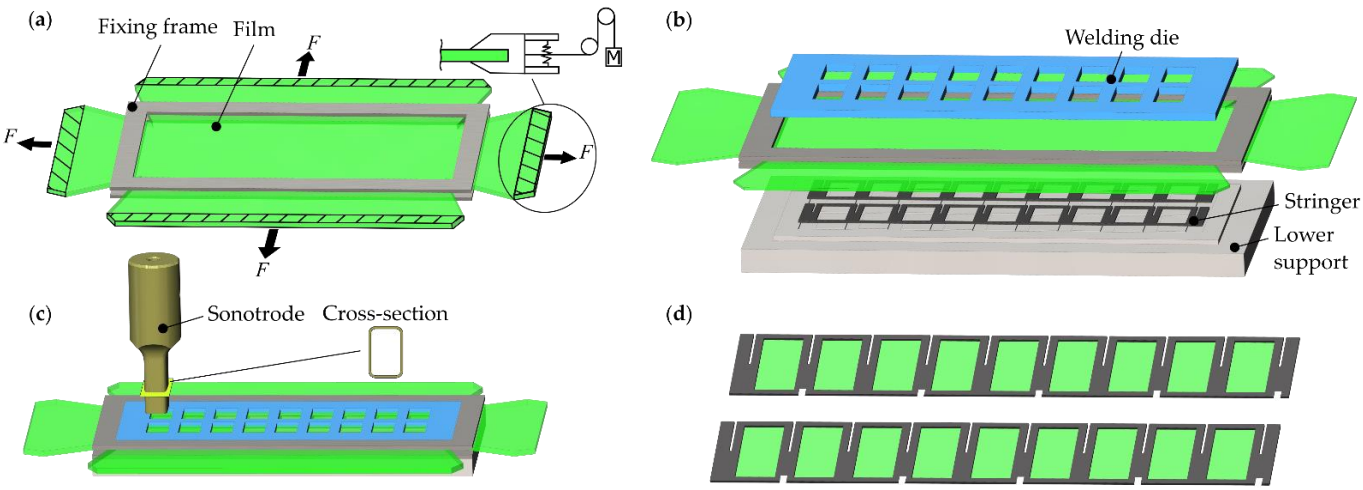

Figure 15. (**a**) Process of pretension the film using a force-controlled set-up including clamps and weights and the subsequent conservation of the resulting stress state by applying a fixing frame, (**b**) necessary components for ultrasonic welding including welding die, lower support carrying the stringers and the pre-tensioned film, (**c**) rectangular sonotrode with its cross-section as well as the final setup for ultrasonic welding of the film and the stringer, (**d**) stringers with attached films.

After removing the excess film material, the curved frame and the stringers are assembled. Finally, the cover layer and the perforated cover sheet are adhesively bonded to the cavity structure (see Figure 16).

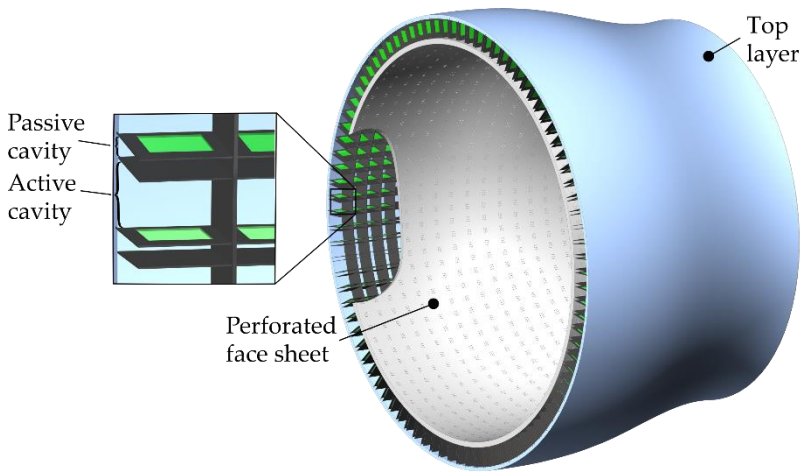

Figure 16. Design study of a curved FHR liner with the perforated face sheet including active and passive cavities, the covering face sheet and the strip slotted cavity structure.

5.2. Design and Manufacturing Concept of Curved PR-Liner

Since the cavities of the PR liner do not have flexible side walls compared to the FHR liner, their manufacturing process is less complex, allowing a reduction in manufacturing steps and higher automation potential. Here, the low cost deep drawing process is a suitable choice for manufacturing the resonator cavities (see Figure 17a). This process enables arbitrary shapes of the resonator cavity and mounting surfaces, e.g., a curved geometry of the resonator bottom matching the targeted design space and the corresponding contour of the top layer of the structure [35,49]. However, due to the curved shape, the process of joining the curved film layer onto the cavity structure is more complex. Since the targeted thermoplastic films have a low stiffness, a form-die is required that sets the shape of the curved liner (see Figure 17b). In order to establish a homogeneous tension state, irregular distribution of friction forces during the deflection process of the film, due to the parabolic

shape of the die, should be reduced to minimum by applying lubricants. The cavities are then adhesively joined to the film, cut and finally attached on the cavity support (see Figure 17c). It should be noted that the film does not adopt a curved shape in the area where it is not connected to the cavity. The cross-section of the liner structure is therefore not circular, but a polygon due to the film's elastic properties. The effects on aerodynamic and fluid mechanical conditions must therefore be considered. In order to incorporate drainage channels, the guard panel and cavity-mounts, the injection molding process is chosen for the manufacturing of the cavity support (see Figure 17). A design concept of the barrel-shaped PR-liner with its main components is shown in Figure 17d. The guard plate is installed on the in-cooperated mounts of the cavity support. Its perforations must be evenly distributed to create homogeneous flow conditions for each resonator. Furthermore, the size of the perforation should be small enough to prevent objects from passing through and damaging the film layer and big enough to prevent blockage. To avoid a reduction of the acoustic performance of the PR-liner, the guard plate should have a perforation percentage of about 30% to achieve acoustical transparency [50,51].

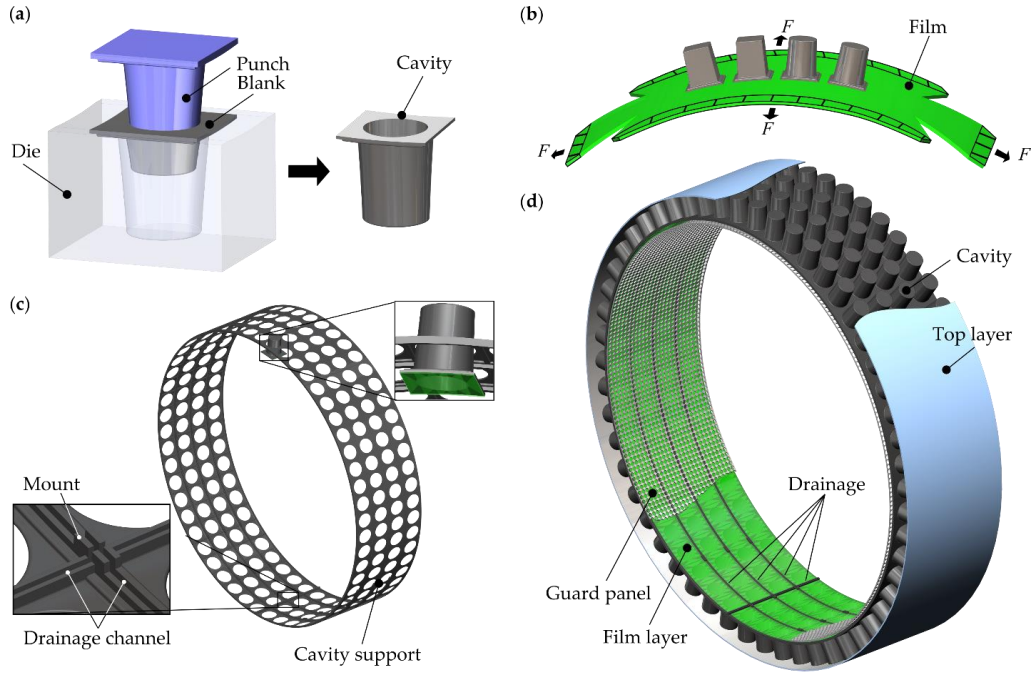

Figure 17. (**a**) Schematic thermoforming process of the resonator cavity, (**b**) joining process of the curved and pre-tensioned film and the cavity, (**c**) cavity support with functional elements such as the drainage channel and mounts for attaching the guard panel, (**d**) design concept of the barrel-shaped PR-liner.

Due to described differential design approach, separating the cavity and the cavity support increases the manual effort for the assembly of the entire liner. An alternative approach to eliminate the assembly process is to combine the two parts in an integral design and manufacture them by injection molding or, for even greater cost efficiency, by rotational thermoforming. However, this approach requires the joining process of the film to be adapted. Since the supports and drainage channels have to be omitted, the film needs to be joined individually for each circularly arranged cell row, requiring high manual effort.

6. Conclusions

Different aspects of two new liner concepts have been addressed in the current study. Both concepts, the Helmholtz Resonator liner with flexible walls (FHR) and the plate resonator concept (PR) make use of material inherent damping for the flexible elements of

the concepts. The following summarizes the conclusions of the four main thematic aspects of the presented study.

6.1. Experimental Investigation

The experimental results show an additional effect in the dissipation of the FHR compared to the established HR. Regarding the acoustical measurements at low frequencies, the TPU films with a rectangular cut-out showed the highest dissipation. The presented experimental results confirm the results of previous numerical studies [17], which indicated that materials with Young's modulus higher than 50 MPa seem to be less suitable for the application in the targeted broadband silencers. The size and position of the back cavity does not seem to have a big effect on the dissipation, implying that the back cavity can be small compared to the resonator.

Further studies will investigate the optimal number of active and passive cells, as well as the optimal position of the passive cells in relation to the active cells. In regards to the dissipation, the relationship between the shape and the area of the flexible wall should be analyzed as well. In further investigations the following topics will be answered, such as the optimal number of active and passive cells. Also, the best position of the passive cells in relation to the active ones will be investigated. In addition, the relationship between the shape and the area of the flexible wall in relation to its dissipation will be analyzed.

6.2. Models and Parameter Studies of FHR/PR Liner

The parameter studies revealed that special care should be taken when selecting adequate materials and geometries to tune the concepts for low-frequency damping. The Young's modulus in combination with the loss factor is a highly influential parameter for both concepts. For the FHR, a low Young's modulus shifts the TL to lower frequencies, and for the PR, it is possible to adjust the attenuation to one or two peaks in the TL spectrum. Additionally, a lower Young's modulus (in combination with a high loss factor) leads to a more broadband peak in the TL curve for the PR liner.

Plate thickness is a parameter that influences the frequency as well as the amplitude of the attenuation for both concepts. For highest attenuation, the plate should be very thin (< 0.2 mm). However, the resonance frequency of the PR liner is lowest with a thick plate. Consequently, there exists a trade-off between highest attenuation and attenuation at the lowest possible frequency for both concepts regarding plate thickness.

The plate dimensions (diameter for FHR, length for PR) alters the frequency of the TL significantly less than the other varied parameters. Still, the results suggest that the plate should be as large as possible for maximum attenuation for both the FHR and PR concept. Thereby, the limiting factor is certainly the installation space.

The height of the cavity (PR), respectively, the second cavity (FHR) has a similar influence as the plate thickness. A higher cavity leads to attenuation at lower frequencies but is limited by the installation space as well. Besides, the concepts differ in the height of the TL. A higher cavity leads to a slightly higher TL for the PR but to a lower TL for the FHR.

These parameter studies revealed the main trends for selected parameters of the Helmholtz resonator concept with flexible walls and the plate resonator. To find an optimal design, however, these parameters need to be varied simultaneously. This is a subject of future investigations.

6.3. Structural Mechanical Analysis

The change of the core structure leads to higher stresses, especially for the face sheet. Therefore, an adjustment was made, using PA6-GF with promising structural–mechanical properties to withstand the occurring static loads. The key issue for the application of the novel acoustic liners in a jet engine is the relation between acoustic efficiency, structural mechanics and total weight of the liner structure. The load relief of the core structure through the application of additional walls with and without cut-outs must be further

optimized. As a result, depending on the distance between the cell walls, the tension in the cut-out bars could be reduced. In this context, a reduction of the weight is possible using thinner core walls made out of PA6-GF. On the contrary, the investigations show that the acoustic behavior is strongly dependent on the tension state of the films. Therefore, the deformation of the frame should be minimal, which stands in contrast to thinner walls and weight reduction. Simultaneously, the aspired load reduction in the upper web leads to a tighter arrangement of the square combs and to an increase of nonfunctional passive cells. Further investigations are necessary to find the optimal parameter settings of the described multidimensional optimization problem.

6.4. Design Concepts and Production

With regard to the manufacturing process of the FHR liner, the introduced process of ultrasonic welding bears the potential to automatize the joining process of the flexible thermoplastic films and the support structure. However, the assembly of the strip-slot design of the cell core requires an excessive amount of manual effort. Here, the adaption of the process introduced by Britzke [52] has the potential to resolve this issue. In contrast, the presented concept of the PR liner allows the application of the cost-efficient deep drawing process, rotational thermoforming or injection molding in dependence of an integral or differential design of the cavities and support structure.

With regard to the design and introduced manufacturing concepts, the integration of the film is the critical process step of both liner principles. Since the tension state of the integrated films affects the performance of the acoustic liners, a concept for reproducible pre-stressing and incorporating the film into the support structure was presented. However, since the targeted material group of thermoplastics and thermoplastic elastomers tends to relaxation, experiments must be carried out to determine the extent of relaxation as a function of deflection force and time in order to predict which tension state the film will attain in the state of operation.

Author Contributions: Conceptualization, M.N.; methodology, M.N., J.G., F.K, V.R., M.P. and K.K.; formal analysis, V.R., F.K., M.P. and M.N.; investigation, M.N., J.G., F.K, V.R., M.P., K.B. and K.K.; writing—original draft preparation, M.N., J.G., F.K, V.R., M.P. and K.B.; writing—review and editing, M.N., J.G., F.K, V.R., M.P., K.B., K.K. and E.S.; visualization, M.N., J.G., F.K, V.R. and M.P.; supervision, N.M., L.E., E.S. and K.H.; project administration, N.M., L.E., E.S., K.K. and K.H.; funding acquisition, N.M., L.E., E.S. and K.H. All authors have read and agreed to the published version of the manuscript.

Funding: Funded by the Deutsche Forschungsgemeinschaft (DFG, German Research Foundation)—416814415, 416728326 and 416728553. The financial support of the work in the framework of the LuFo VI-1 project "FLIER" (Flexible wall structures for acoustic LINERs) by the Federal Ministry for Economic Affairs and Climate Action (contract numbers: 20E1915A, 20E1915B and 20E1915C), based on a decision of the German Bundestag, is gratefully acknowledged.

Institutional Review Board Statement: Not applicable.

Informed Consent Statement: Not applicable.

Data Availability Statement: The data presented in the current study are available on request from the corresponding author.

Conflicts of Interest: The authors declare no conflict of interest.

References

1. Mi, Y.; Yu, X. Attenuation of low-frequency sound in U-shaped duct with membrane coupled acoustic resonator: Modeling and analysis. *J. Sound Vib.* **2020**, *489*, 115679. [CrossRef]
2. Wu, D.; Zhang, N.; Mak, C.M.; Cai, C. Hybrid noise control using multiple Helmholtz resonator arrays. *Appl. Acoust.* **2019**, *143*, 31–37. [CrossRef]
3. Jones, M.; Howerton, B.; Ayle, E. Evaluation of Parallel-Element, Variable-Impedance, Broadband Acoustic Liner Concepts. In Proceedings of the 18th AIAA/CEAS Aeroacoustics Conference (33rd AIAA Aeroacoustics Conference), Colorado Springs, CO, USA, 4–6 June 2012; American Institute of Aeronautics and Astronautics: Reston, VI, USA, 2012. ISBN 978-1-60086-932-7.

4. Jones, M.G.; Nark, D.M.; Howerton, B.M. Impedance eduction for uniform and multizone acoustic liners. *Int. J. Aeroacoustics* **2021**, *20*, 458–477. [CrossRef]
5. Dodge, C.; Zhang, Y.; Cattafesta, L.N.; Howerton, B.M.; Kreitzman, J.R. A Dielectric Elastomer Acoustic Liner. In Proceedings of the AIAA Aviation 2021 Forum, Virtual Event, 2–6 August 2021; American Institute of Aeronautics and Astronautics: Reston, VI, USA, 2021. ISBN 978-1-62410-610-1.
6. Horowitz, S.B.; Sheplak, M.; Cattafesta, L.N.; Nishida, T. A MEMS acoustic energy harvester. *J. Micromech. Microeng.* **2006**, *16*, S174–S181. [CrossRef]
7. De Bedout, J.M.; Franchek, M.A.; Bernhard, R.J.; Mongeau, L. Adaptive-passive noise control with self-tuning Helmholtz resonators. *J. Sound Vib.* **1997**, *202*, 109–123. [CrossRef]
8. Hu, G.; Tang, L.; Cui, X. On the modelling of membrane-coupled Helmholtz resonator and its application in acous-tic metamaterial system. *Mech. Syst. Signal Process.* **2019**, *132*, 595–608. [CrossRef]
9. Kohlenberg, F.; Schulz, A.; Enghardt, L.; Knobloch, K. Modelling of Acoustic Liners Consisting of Helmholtz Reso-nators Coupled with a Second Cavity by Flexible Walls. In Proceedings of the 28th AI-AA/CEAS Aeroacoustics 2022 Conference, Southampton, UK, 14–17 June 2022; American Institute of Aeronautics and Astronautics: Reston, VI, USA, 2022. ISBN 978-1-62410-664-4.
10. Wang, C.; Cheng, L.; Huang, L. Realization of a broadband low-frequency plate silencer using sandwich plates. *J. Sound Vib.* **2008**, *318*, 792–808. [CrossRef]
11. Liu, G.; Zhao, X.; Zhang, W.; Li, S. Study on plate silencer with general boundary conditions. *J. Sound Vib.* **2014**, *333*, 4881–4896. [CrossRef]
12. Kisler, R.; Sarradj, E. Plate Silencers for Broadband Low Frequency Sound Attenuation. *Acta Acust. United Acust.* **2018**, *104*, 521–527. [CrossRef]
13. Fuchs, H.V. *Applied Acoustics: Concepts, Absorbers, and Silencers for Acoustical Comfort and Noise Control. Alternative Solutions-Innovative Tools-Practical Examples*; Springer: Berlin/Heidelberg, Germany, 2013; ISBN 9783642293665.
14. Huang, L. A theoretical study of duct noise control by flexible panels. *J. Acoust. Soc. Am.* **1999**, *106*, 1801–1809. [CrossRef]
15. Huang, L. Broadband sound reflection by plates covering side-branch cavities in a duct. *J. Acoust. Soc. Am.* **2006**, *119*, 2628–2638. [CrossRef]
16. Wang, C.; Huang, L. Analysis of absorption and reflection mechanisms in a three-dimensional plate silencer. *J. Sound Vib.* **2008**, *313*, 510–524. [CrossRef]
17. Neubauer, M.; Schwaericke, F.; Radmann, V.; Sarradj, E.; Modler, N.; Dannemann, M. Material Selection Process for Acoustic and Vibration Applications Using the Example of a Plate Resonator. *Materials* **2022**, *15*, 2935. [CrossRef] [PubMed]
18. Hähnel, F.; Wolf, K. Evaluation of the Material Properties of Resin-impregnate NOMEX® Paper as Basis for the Simulation of the Impact Behaviour of Honeycomb Sandwich. In Proceedings of the 3rd International Conference on Composite Testing and Model Identification, Porto, Portugal, 10 April 2006.
19. Foo, C.C.; Chai, G.B.; Seah, L.K. Mechanical properties of Nomex material and Nomex honeycomb structure. *Compos. Struct.* **2007**, *80*, 588–594. [CrossRef]
20. Seemann, R.; Krause, D. Analysis of Free Edge Stresses in Composite Laminates Using Higher Order Theories. *Indian J. Mater. Sci.* **2014**, *2014*, 15.
21. Zhang, Y.; Liu, T.; Tizani, W. Experimental and numerical analysis of dynamic compressive response of Nomex honeycombs. *Compos. Part B Eng.* **2018**, *148*, 27–39. [CrossRef]
22. Giglio, M.; Manes, A.; Gilioli, A. Investigations on sandwich core properties through an experimental–numerical approach. *Compos. Part B Eng.* **2012**, *43*, 361–374. [CrossRef]
23. Liu, L.; Meng, P.; Wang, H.; Guan, Z. The flatwise compressive properties of Nomex honeycomb core with debond-ing imperfections in the double cell wall. *Compos. Part B Eng.* **2015**, *76*, 122–132. [CrossRef]
24. Neubauer, M.; Dannemann, M.; Kucher, M.; Bleil, N.; Wollmann, T.; Modler, N. Numerical Buckling Analysis of Hybrid Honeycomb Cores for Advanced Helmholtz Resonator Liners. *J. Compos. Sci.* **2021**, *5*, 116. [CrossRef]
25. Heimbs, S.; Middendorf, P.; Hampf, C.; Hähnel, F.; Wolf, K. Aircraft Sandwich Structures with Folded Core under Impact Load Porta (PRT). In Proceedings of the 8th International Conference on Sandwich Structures, ICSS8, Porto, Portugal, 6 May 2008; pp. 369–380.
26. Wang, B.; Hu, J.; Li, Y.; Yao, Y.; Wang, S.; Ma, L. Mechanical properties and failure behavior of the sandwich struc-tures with carbon fiber-reinforced X-type lattice truss core. *Compos. Struct.* **2018**, *185*, 619–633. [CrossRef]
27. Côté, F.; Russell, B.P.; Deshpande, V.S.; Fleck, N.A. The Through-Thickness Compressive Strength of a Composite Sandwich Panel with a Hierarchical Square Honeycomb Sandwich Core. *J. Appl. Mech.* **2009**, *76*, 061004. [CrossRef]
28. Ma, X.; Su, Z. Development of acoustic liner in aero engine: A review. *Sci. China Technol. Sci.* **2020**, *63*, 2491–2504. [CrossRef]
29. Pütz, M.; Lafont, U.; Wittlich, M.; Markestein, E.; Herrmann, C.; Fischer, H. 3D honeycomb for advanced manufacturing for space application. *CEAS Space J.* **2022**, 1–9. [CrossRef]
30. Zhao, Z.; Liu, C.; Wang, H.; Simon, J.-W.; Wang, J.; Li, Y. Crushing behavior of curved Nomex honeycombs under combined shear-compression loads. *Int. J. Mech. Sci.* **2022**, *228*, 107480. [CrossRef]
31. Wadley, H.N.G. Multifunctional periodic cellular metals. *Philos. Trans. A Math. Phys. Eng. Sci.* **2006**, *364*, 31–68. [CrossRef] [PubMed]

32. Dannemann, M.; Kucher, M.; Kunze, E.; Modler, N.; Knobloch, K.; Enghardt, L.; Sarradj, E.; Höschler, K. Experimental Study of Advanced Helmholtz Resonator Liners with Increased Acoustic Performance by Utilising Material Damping Effects. *Appl. Sci.* **2018**, *8*, 1923. [CrossRef]
33. Dahiya, A.K.; Bhuyan, B.K.; Kumar, S. Perspective study of abrasive water jet machining of composites—A review. *J. Mech. Sci. Technol.* **2022**, *36*, 213–224. [CrossRef]
34. Khan, M.A.; Soni, H.; Mashinini, P.M.; Uthayakumar, M. Abrasive water jet cutting process form machining metals and composites for engineering applications: A review. *Eng. Res. Express* **2021**, *3*, 22004. [CrossRef]
35. Atul, S.T.; Babu, M.C.L. A review on effect of thinning, wrinkling and spring-back on deep drawing process. *Proc. Inst. Mech. Eng. Part B J. Eng. Manuf.* **2019**, *233*, 1011–1036. [CrossRef]
36. Goergen, C.; Schommer, D.; Duhovic, M.; Mitschang, P. Deep drawing of organic sheets made of hybrid recycled carbon and thermoplastic polyamide 6 staple fiber yarns. *J. Thermoplast. Compos. Mater.* **2020**, *33*, 754–778. [CrossRef]
37. Bhudolia, S.K.; Gohel, G.; Leong, K.F.; Islam, A. Advances in Ultrasonic Welding of Thermoplastic Composites: A Review. *Materials* **2020**, *13*, 1284. [CrossRef] [PubMed]
38. Villegas, I.F. Ultrasonic Welding of Thermoplastic Composites. *Front. Mater.* **2019**, *6*, 291. [CrossRef]
39. Liu, S.-J.; Chang, I.-T. Optimizing the Weld Strength of Ultrasonically Welded Nylon Composites. *J. Compos. Mater.* **2002**, *36*, 611–624. [CrossRef]
40. Liu, S.-J.; Chang, I.-T.; Hung, S.-W. Factors affecting the joint strength of ultrasonically welded polypropylene composites. *Polym. Compos.* **2001**, *22*, 132–141. [CrossRef]
41. Knobloch, K.; Enghardt, L.; Bake, F. Helmholtz Resonator Liner with Flexible Walls. In Proceedings of the 2018 AIAA/CEAS Aeroacoustics Conference, Atlanta, Georgia, 25–29 June 2018; American Institute of Aeronautics and Astronautics: Reston, VI, USA, 2018. ISBN 978-1-62410-560-9.
42. Wang, C.; Han, J.; Huang, L. Optimization of a clamped plate silencer. *J. Acoust. Soc. Am.* **2007**, *121*, 949–960. [CrossRef] [PubMed]
43. Wang, C. Development of a Broadband Silencer in Flow duct. Ph.D. Thesis, Hong Kong Polytechnic University, Hong Kong, China, 2008.
44. Choy, Y.S.; Liu, Y.; Cheung, H.Y.; Xi, Q.; Lau, K.T. Development of composite plate for compact silencer design. *J. Sound Vib.* **2012**, *331*, 2348–2364. [CrossRef]
45. Azimi, M.; Ommi, F.; Alashti, N.J. Using Acoustic Liner for Fan Noise Reduction in Modern Turbofan Engines. *Int. J. Aeronaut. Space Sci.* **2014**, *15*, 97–101. [CrossRef]
46. Özkaya, E.; Gauger, N.R.; Hay, J.A.; Thiele, F. Efficient Design Optimization of Acoustic Liners for Engine Noise Reduction. *AIAA J.* **2020**, *58*, 1140–1156. [CrossRef]
47. Tsai, S.W.; Wu, E.M. A General Theory of Strength for Anisotropic Materials. *J. Compos. Mater.* **1971**, *5*, 58–80. [CrossRef]
48. Hoeschler, K.; Sarradj, E.; Modler, N.; Enghardt, L. Novel Jet Engine Acoustic Liner with Improved Broadband Noise Absorption. In Proceedings of the 31st Congress of the International Council of the Aeronautical Sciences, ICAS 2018, Belo Horizonte, Brazil, 9–14 September 2018; International Council of The Aeronautical Sciences (ICAS): Bonn, Germany, 2018. ISBN 978-393218288-4.
49. Gherissi, A.; Abbassi, F.; Ammar, A.; Zghal, A. Numerical and Experimental Investigations on Deep Drawing of G1151 Carbon Fiber Woven Composites. *Appl. Compos. Mater.* **2016**, *23*, 461–476. [CrossRef]
50. Mechel, F.P. *Schallabsorber Band II: Innere Schallfelder—Strukturen*; S. Hirzel: Stuttgart/Leipzig, Germany, 1995; ISBN 978-3-7776-0572-2.
51. Schirmer, W. *Technischer Lärmschutz*; Springer: Berlin/Heidelberg, Germany, 2006; ISBN 978-3-540-25507-9.
52. Britzke, M. Verfahren zur automatisierten Fertigung rahmenloser Sandwichplatten mit Papierwabenkern. *Light Des.* **2009**, *2*, 55–62. [CrossRef]